Optimized Complementary Waveform Subsets within an FM Noise Radar CPI

Charles A. Mohr, Patrick M. McCormick, Shannon D. Blunt
Radar Systems Lab (RSL), University of Kansas, Lawrence, KS

***Abstract*—Complementary codes are known to provide theoretically zero sidelobes under the conditions of zero Doppler and an ideal (distortion-free) transmitter. In contrast, the design of complementary FM (Comp-FM) waveforms is demonstrated here using gradient-based optimization of polyphase-coded FM (PCFM). It is shown that these waveforms are inherently more robust to Doppler than codes and, being FM, are also naturally amenable to high-power transmitters.**

Further, distinct subsets of complementary waveforms are used in the coherent processing interval (CPI) of FM noise radar where they can be pre-summed on receive to reduce the overall sidelobe level. Because each subset is different, the presence of non-zero Doppler and/or transmitter distortion cause the rate of sidelobe reduction to revert to that achieved by FM noise radar, which is still linear with the number of pulses. The performance of these complementary waveforms is demonstrated in simulation and through free-space experimental measurements.

Keywords—complementary waveforms, FM noise radar

I. Introduction

Complementary codes were first formulated by Golay in 1961 [1]. Since then numerous variants have been developed (e.g. [2-7]). When modulated onto radar pulses, complementary codes have the unique ability to completely suppress autocorrelation sidelobes when their autocorrelations are coherently combined. Despite this desirable characteristic, the actual use of these codes has remained limited for radar applications due to issues that are fundamentally a function of fidelity.

First, it is known that the sidelobe suppression capability of complementary codes degrades rather rapidly in the presence of Doppler [8]. This result is not surprising since Doppler in this context is essentially a mismatch to the expected sidelobe structures that otherwise perfectly cancel when combined. Bearing this effect in mind, there have been efforts to improve the robustness to Doppler for complementary codes [9-14]. The other issue is the unavoidable distortion that the transmitter imposes on all waveforms and is particularly deleterious for codes when implemented as continuous waveforms (see [15,16]). Like Doppler distortion, the resulting deviation from the theoretical code structure caused by the transmitter induces a mismatch that limits sidelobe cancellation.

To address these effects we consider the design of complementary FM (Comp-FM) waveforms whose physical structure are naturally amenable to high-power radar transmitters and thus experience minimal distortion. Subsets of these waveforms are optimized using a polyphase-coded FM (PCFM) structure [15] according to a gradient-based formulation [17,18] that provides both good spectral containment and realizes a degree of complementary sidelobe-cancelling capability when combined. Moreover, as part of an overall FM noise radar framework (see [19-21] for details on FM noise waveforms), each subset contains a unique group of waveforms that are not repeated. As such, the inevitable degradation due to Doppler and transmitter effects is tempered by the incoherent combination of unique sidelobes for FM noise radar in which the decrease is linear with the number of pulses.

It is shown in simulation that these Comp-FM waveforms do not achieve perfect sidelobe cancellation for zero-Doppler, but do degrade more gracefully as Doppler increases. Within the FM noise radar context they are also demonstrated experimentally to provide significant practical sidelobe cancellation.

II. Waveform Representation

Consider a pulsed, FM waveform $s(t)$ defined on $t \in [0, T]$ for pulsewidth T according to the first-order PCFM model [15]

$$s(t;\mathbf{x}) = \exp\left\{ j\left(\int_0^t g(\tau) * \left[\sum_{n=1}^{N} \alpha_n \, \delta\big(\tau-(n-1)T_{\mathrm{p}}\big) \right] d\tau \right) \right\} \quad (1)$$
$$= \exp\{ j\phi(t) \} .$$

Here $g(t)$ is a shaping filter with time support $[0, T_{\mathrm{p}}]$, the operation $*$ is convolution, $\delta(t)$ is an impulse function, and $\mathbf{x} = [\, \alpha_1 \;\; \alpha_2 \cdots \alpha_N \,]^T$ contains the N parameters to optimize. Because it is composed of linear operations, the phase function in (1) can also be expressed as

$$\phi(t) = \sum_{n=1}^{N} b_n(t)\, \alpha_n \, , \quad (2)$$

where

$$b_n(t) = \int_0^t g(\tau-(n-1)T_p)\, d\tau \quad (3)$$

is the continuous basis function that is weighted by α_n. Here we assume that $g(t)$ is a rectangular filter so that the basis functions of (3) are time-shifted ramp functions.

For optimization, a discretization of the PCFM model is

$$\mathbf{s} = \exp(j\mathbf{B}\mathbf{x}) \quad (4)$$

in which the columns of the $M \times N$ matrix $\mathbf{B}$ are discretized versions of $b_n(t)$ and $M = KN$ is the length of $\mathbf{s}$ in samples, for K the "over-sampling" factor relative to 3-dB bandwidth B. Note that N approximates the time-bandwidth product BT [15] for each individual waveform.

This work was supported by the Office of Naval Research under Contract #N00014-16-C-2029. DISTRIBUTION STATEMENT A. Approved for Public Release.

III. Complementary Waveform Optimization

Parameterize the zth discretized waveform $\mathbf{s}_z$ using $\mathbf{x}_z$ according to the model in (4). We thus wish to design $\mathbf{x}_z$ for $z = 1, \ldots, Z$ such that the coherent combination of the autocorrelations of $s(t; \mathbf{x}_z)$ generated by (1) produces a minimal sidelobe response (ideally zero). Append $M-1$ zeros to $\mathbf{s}_z$ as

$$\overline{\mathbf{s}}_z = [\mathbf{s}_z^T \ \mathbf{0}_{1\times(M-1)}]^T \tag{5}$$

such that the $(2M-1)\times 1$ discretized frequency response is

$$\overline{\mathbf{s}}_{\mathrm{f},z} = \mathbf{A}^H \overline{\mathbf{s}}_z \tag{6}$$

for $\mathbf{A}^H$ the $(2M-1)\times(2M-1)$ DFT matrix and $\mathbf{A}$ the inverse DFT. The $(2M-1)\times 1$ discretized aggregate autocorrelation for the subset of Z waveforms can therefore be written as

$$\mathbf{r} = \left[r_{-M+1} \ \cdots \ r_0 \ \cdots \ r_{M-1}\right]^T = \sum_{z=1}^{Z} \mathbf{A}\left(\overline{\mathbf{s}}_{\mathrm{f},z} \odot \overline{\mathbf{s}}_{\mathrm{f},z}^{*}\right), \tag{7}$$

for $(\bullet)^*$ complex conjugation and $\odot$ the Hadamard product.

To minimize the sidelobes of (7), we use the generalized integrated sidelobe level (GISL) metric from [17] that operates on the p-norm ratio of the sidelobes to the mainlobe and subsumes both ISL ($p = 2$) and PSL ($p = \infty$). Therefore the cost function is [17]

$$J = \frac{\left\|\mathbf{w}_{\mathrm{SL}} \odot \mathbf{r}\right\|_p}{\left\|\mathbf{w}_{\mathrm{ML}} \odot \mathbf{r}\right\|_p}, \tag{8}$$

where $\|\bullet\|_p$ is the p-norm and the $(2M-1)\times 1$ vectors $\mathbf{w}_{\mathrm{SL}}$ and $\mathbf{w}_{\mathrm{ML}}$ extract the sidelobes and mainlobe of autocorrelation $\mathbf{r}$. For an "over-sampling" factor of K, the null-to-null width of the mainlobe comprises the $2K-1$ samples in the center of $\mathbf{r}$, with $\mathbf{w}_{\mathrm{SL}}$ and $\mathbf{w}_{\mathrm{ML}}$ constructed accordingly. It was shown in [18] that setting the mainlobe width in this manner likewise effectively establishes the 3-dB bandwidth.

The $N\times 1$ gradient vector for the zth waveform in the complementary subset is defined as

$$\nabla_{\mathbf{x}_z} = \left[\frac{\partial}{\partial\alpha_{1,z}} \quad \frac{\partial}{\partial\alpha_{2,z}} \quad \cdots \quad \frac{\partial}{\partial\alpha_{N,z}}\right]^T, \tag{9}$$

which contains a partial derivative with respect to each of the N parameters of the zth waveform. The gradient of cost function (8) using (9) can then be expressed as

$$\nabla_{\mathbf{x}_z} J = 2\overline{\mathbf{B}}^T \Im\left\{\overline{\mathbf{s}}_z^{*} \odot \left(\mathbf{A}\left[\overline{\mathbf{s}}_{\mathrm{f},z} \odot \left\{\mathbf{A}^H\left(\mathbf{w}_{\mathrm{T}} \odot \mathbf{d} \odot \mathbf{r}\right)\right\}\right]\right)\right\} \tag{10}$$

where the matrix $\mathbf{B}$ has likewise been appended with $M-1$ rows of zeros as

$$\overline{\mathbf{B}} = \left[\mathbf{B}^T \ \mathbf{0}_{N\times(M-1)}\right]^T, \tag{11}$$

$\Im\{\bullet\}$ is the imaginary part of the argument, and the $(2M-1)\times 1$ vectors that are Hadamard multiplied to $\mathbf{r}$ are

$$\mathbf{d} = \left[\left|r_{-M+1}\right|^{p-2} \ \cdots \ \left|r_0\right|^{p-2} \ \cdots \ \left|r_{M-1}\right|^{p-2}\right]^T \tag{12}$$

and

$$\mathbf{w}_{\mathrm{T}} = \frac{\left\|\mathbf{w}_{\mathrm{SL}} \odot \mathbf{r}\right\|_p}{\left\|\mathbf{w}_{\mathrm{ML}} \odot \mathbf{r}\right\|_p}\left[\left(\frac{1}{\left\|\mathbf{w}_{\mathrm{SL}} \odot \mathbf{r}\right\|_p^p}\right)\mathbf{w}_{\mathrm{SL}} - \left(\frac{1}{\left\|\mathbf{w}_{\mathrm{ML}} \odot \mathbf{r}\right\|_p^p}\right)\mathbf{w}_{\mathrm{ML}}\right]. \tag{13}$$

Expressed in this manner, the gradient in (10) can be computed using fast Fourier transforms (FFTs) and vector/matrix multiplies that can be efficiently implemented [23,24].

The generic descent optimization update for $\mathbf{x}_z$ at the ith iteration is

$$\mathbf{x}_{z,i+1} = \mathbf{x}_{z,i} + \mu_{z,i}\mathbf{p}_{z,i} \tag{14}$$

where $\mathbf{p}_{z,i}$ is the current descent direction for the zth waveform and $\mu_{z,i}$ is the associated step-size. Here, the descent direction is updated using the heavy-ball gradient descent method [25] that uses a combination of the current and past gradients and is known to converge faster than standard gradient descent. The heavy-ball descent direction at the ith iteration is defined as

$$\mathbf{p}_{z,i} = \begin{cases} -\nabla_{\mathbf{x}_{z,i}} J & \text{when } i = 0 \\ -\nabla_{\mathbf{x}_{z,i}} J + \beta\mathbf{p}_{z,i-1} & \text{otherwise} \end{cases} \tag{15}$$

for $0 \le \beta < 1$. Here the step-size is chosen using a back-tracking method [26].

IV. Simulation Results

A total of 200 subsets of $Z = 5$ complementary waveforms (for a total of $L = 1000$ waveforms) were optimized. These waveforms have a 3-dB bandwidth of $B = 66.7$ MHz and a pulsewidth of $T = 4.5$ μs, and thus each waveform has a time-bandwidth product of $BT = 300$.

Each waveform was initialized with a randomly generated parameter vector $\mathbf{x}$ whose values were drawn from a uniform distribution on $[-\pi, +\pi]$. Each complementary waveform subset was optimized for 10^4 iterations. These optimized subsets are compared with the pseudo-random optimized (PRO) FM noise waveforms from [20]. For this comparison it is useful to define the notions of *complementary sidelobe cancellation* (CSC) and *incoherent sidelobe cancellation* (ISC), where the former is the amount of reduction provided by complementary waveforms and the latter is the amount of reduction enabled by the averaging of incoherent sidelobes.

Figure 1 illustrates the difference between the CSC, which is unique to complementary waveforms, and the ISC associated with any type of pulse-agile waveform (including FM noise). Individually, an arbitrary complementary waveform has a noticeably higher sidelobe level than an arbitrary PRO-FM waveform. In Fig. 1, this difference is observed to be as much as 20 dB. However, when a subset of five Comp-FM waveforms are jointly optimized and combined, the resulting CSC is nearly 40 dB. In contrast, when combining five PRO-FM waveforms the ISC is 7 dB, which is 10 $\log_{10}$ (5).

The 7 dB sidelobe cancellation can be improved further by simply combining more PRO-FM waveforms, where L unique waveforms provide an ISC of 10 $\log_{10}$ (L). For complementary waveform subsets in this FM noise radar context, with the degree of CSC (in dB) dependent on the optimization, any additional sidelobe cancellation is likewise accrued as ISC

across the number of waveform subsets (e.g. via Doppler processing). Thus the total sidelobe cancellation when combining (L/Z) unique complementary subsets of Z waveforms each is CSC + 10 $\log_{10}$ (L/Z).

Figure 2 demonstrates this CSC-ISC relationship for the coherent integration of $L = 1000$ PRO-FM waveforms versus the coherent integration of $L/Z = 200$ unique subsets of $Z = 5$ complementary waveforms each. Compared to the single PRO-FM waveform from Fig. 1, the ISC = 30 dB of sidelobe suppression is also observed in Fig. 2. For the complementary waveform subsets, the CSC is again about 35 dB, while 10 $\log_{10}$ (200) = 23 dB, thus realizing 58 dB of overall sidelobe suppression, which is likewise evident in Fig. 2. It should be noted, however, that both cases produce the same smaller shoulder lobes at around −70 dB very close to the mainlobe.

Additionally, Comp-FM waveform subsets have been found to produce a mean power spectral density (PSD) similar to that imposed upon PRO-FM waveforms despite no explicit spectral shaping of the former. In Fig. 3, the Comp-FM mean PSD is slightly wider in the passpand, slightly narrower in the roll-off region, and essentially levels off around −20 dB relative to the peak. Given the excellent sidelobe suppression of Comp-FM subsets, it makes sense that the mean PSD would be approximately Gaussian like PRO-FM [19].

Finally, to demonstrate the degree of Doppler tolerance for these Comp-FM waveforms, comparisons are made relative to a 256-chip complementary code set of two and a 256-chip complementary code set of four based on a PONS construction [27]. These codes were oversampled by a factor of three relative to 3-dB bandwidth. Likewise, Comp-FM sets of two and four waveforms were optimized for 10^4 iterations, with each parameterizing vector $\mathbf{x}$ in (1) comprised 256 values and $K = 3$. The peak sidelobe level (PSL) of each complementary set was then calculated as a function of pulse-to-pulse Doppler shift. These results are plotted in Fig. 4, where the most significant PSL changes clearly occur near zero Doppler, with the initially superior PONS complementary codes quickly degrading beyond the Comp-FM waveforms that degrade more gradually. Note that the results in Fig. 4 only consider the sidelobes as a function of CSC. Even with Doppler degradation, Comp-FM waveforms benefit from ISC in addition to the given CSC level due to their non-repeating pulse-agile nature.

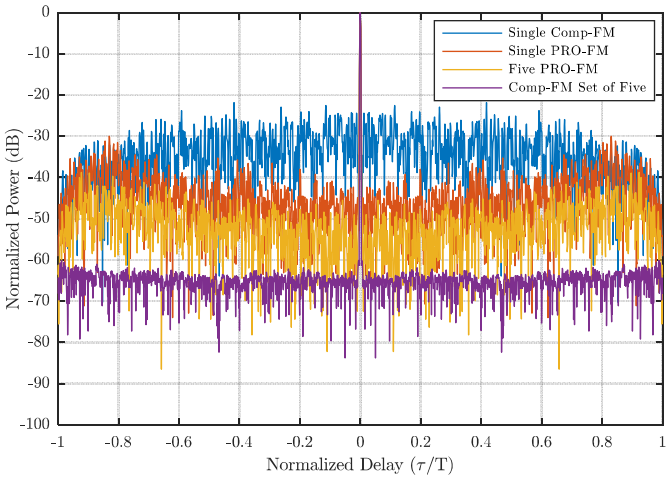

Fig. 1. Simulated autocorrelations for a single Comp-FM waveform, a single PRO-FM waveform, the coherent sum of the autocorrelations of 5 PRO-FM waveforms, and the coherent sum of a Comp-FM subset of 5 waveforms.

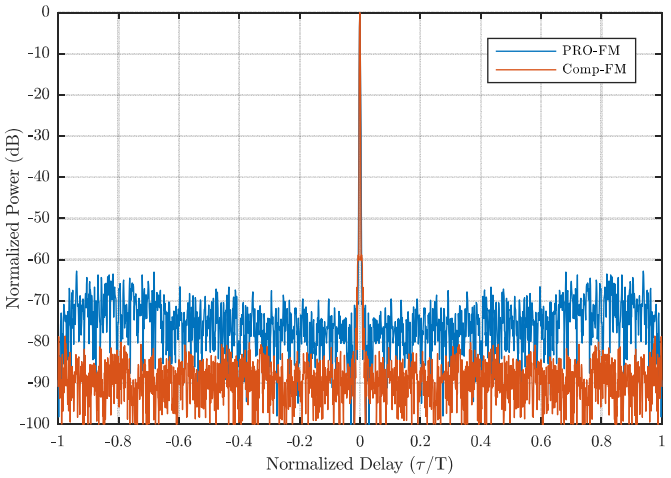

Fig. 2. Simulated coherent sum of autocorrelations for 1000 unique PRO-FM waveforms and for 200 unique Comp-FM subsets of 5 waveforms.

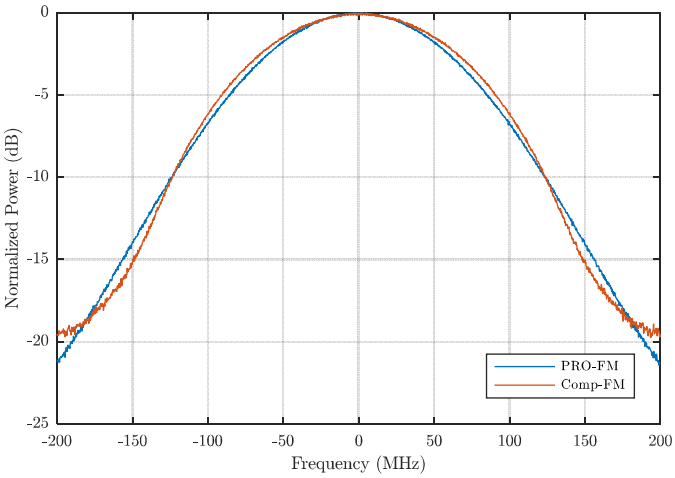

Fig. 3. The mean power spectral density (PSD) for 1000 unique PRO-FM waveforms and for 200 unique Comp-FM subsets of 5 waveforms.

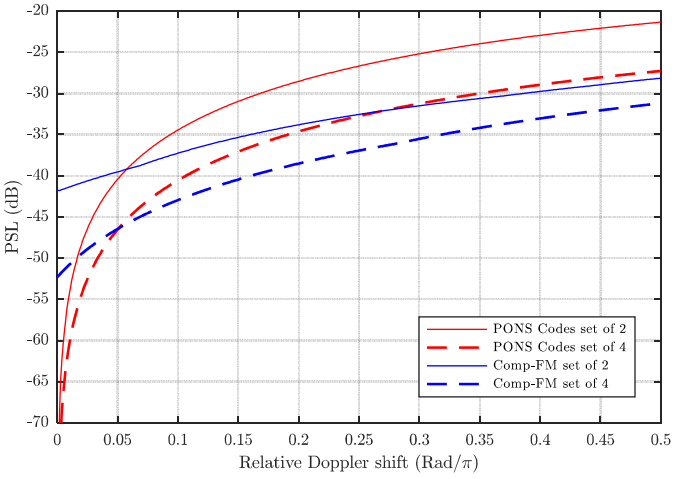

Fig. 4. PSL vs. Doppler for 2 and 4 PONS complementary codes compared to 2 and 4 optimized Comp-FM waveforms.

V. Experimental Results

A concern that typically arises with complementary coded waveforms is how well can their theoretical benefit be realized in practice. To assess how well these Comp-FM waveforms perform in real-world conditions, they were evaluated on hardware in a loopback configuration and an open-air setting.

A. Loopback Assessment

The same L = 1000 Comp-FM and PRO-FM waveforms from the previous section were generated at a center frequency of 3.55 GHz with a pulse repetition frequency (PRF) of 20 kHz and a coherent processing interval of 50 ms. The waveforms were produced using a Tektronix AWG70002A arbitrary waveform generator possessing a 10-bit depth, "transmitted" with a class A amplifier, and then directly connected to an attenuator, followed by a receiver low-noise amplifier, and finally captured with a Rhode & Schwarz FSW26 spectrum analyzer at baseband at a rate of 200 Msamples/s.

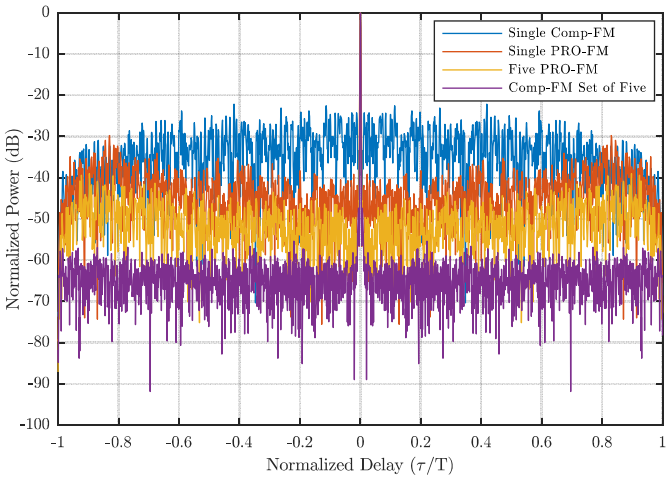

Fig. 5. Loopback measured autocorrelations for a single Comp-FM waveform, a single PRO-FM waveform, the coherent sum of the autocorrelations of 5 PRO-FM waveforms, and the coherent sum of a Comp-FM subset of 5 waveforms.

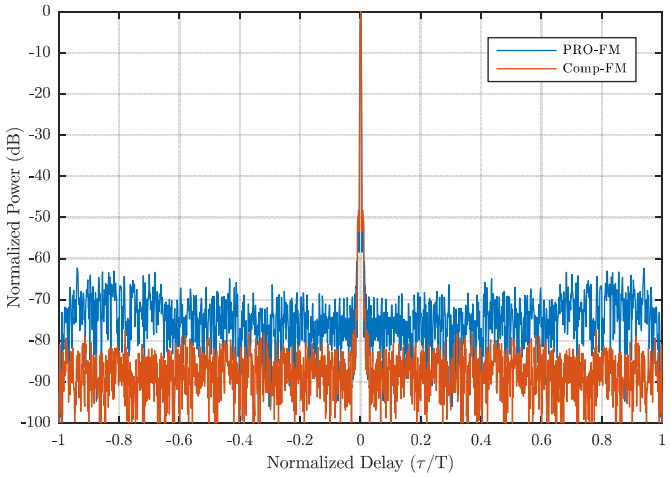

Fig. 6. Loopback measured coherent sum of autocorrelations for 1000 unique PRO-FM waveforms and for 200 unique Comp-FM subsets of 5 waveforms.

Figure 5 shows loopback captured versions of the waveforms depicted in Fig. 1. In each case the sidelobes have risen by a couple dB. However, the amount of complementary sidelobe cancellation (CSC) is still nearly 35 dB. Likewise, Fig. 6 is a direct comparison to Fig. 2. Once again the overall sidelobe levels have increased by about 1-2 dB in places yet the overall amount of sidelobe cancellation is unchanged, with Comp-FM still about 15-20 dB lower than PRO-FM.

B. Open-Air Measurements – Range Profile

These same subsets of waveforms were also transmitted in an open-air setting. The B = 66.7 MHz bandwidth provides a range resolution of 2.5 m, the 50 ms CPI corresponds to a velocity resolution of 0.85 m/s, and the 20 kHz PRF yields an unambiguous range of 7.5 km. On receive, each subset of five waveforms was pre-summed, thus reducing the effective PRF to 4 kHz, which corresponds to an unambiguous velocity of ±84.5 m/s.

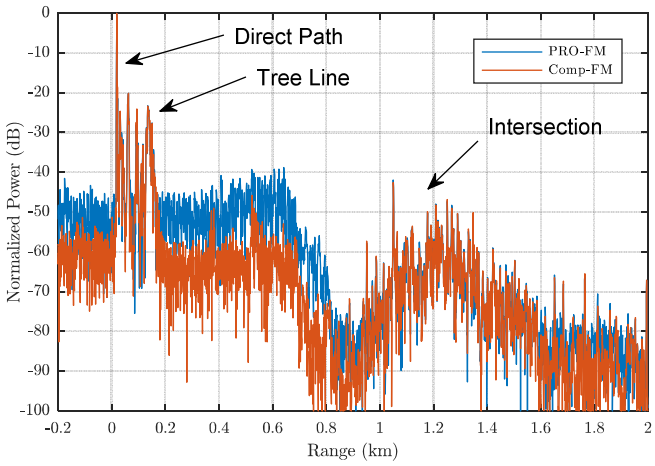

Fig. 7. Measured range profile for 200 repetitions of five unique PRO-FM waveforms and 200 repetitions of one Comp-FM subset of five waveforms

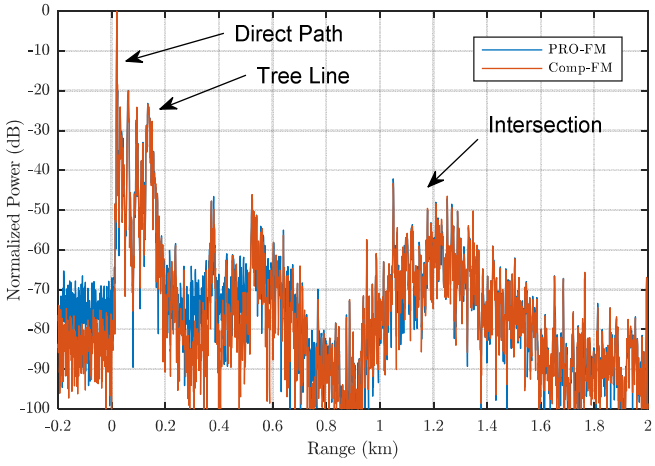

Fig. 8. Measured range profile for 1000 unique PRO-FM waveforms and 200 unique Comp-FM subsets of five.

The measurements were collected from the roof of Nichols Hall on the University of Kansas campus. Separate transmit and receive antennas were pointed towards the intersection of 23rd and Iowa streets, which allowed for the observation of multiple moving vehicles along with several stationary scatterers such as trees and buildings. To illustrate the benefits of waveform uniqueness, we also consider the impact of 200 repetitions of the same Comp-FM subset of five waveforms.

Figure 7 shows measured range profiles for 200 repetitions of five unique PRO-FM waveforms and 200 repetitions of one Comp-FM subset of five waveforms, for a CPI of 1000 pulses in each case. The most noticeable difference is in the vicinity of the direct path component, where the Comp-FM case yields sidelobes that are roughly 10-15 dB lower than the PRO-FM case.

Compare this result with that in Fig. 8 for 1000 unique PRO-FM waveforms and 200 unique Comp-FM subsets of five. In the vicinity of the direct path component, an additional 15-20 dB of sidelobe suppression is realized for both cases, which has revealed multiple smaller scatterers in the 0.4 to 0.6 km range.

C. *Open-Air Measurements – Doppler Processing*

Now consider the viability of these waveforms in the context of Doppler processing for the same field of view (intersection of 23rd and Iowa streets in Lawrence, KS). The same waveforms/data used to produce Figs. 7 and 8 above was Doppler processed using a Hamming window and simple projection-based clutter cancellation (since the platform is stationary). The results in Figs. 9-12 were collected in four consecutive CPIs.

Figures 9 and 10 depict the range-Doppler responses for 200 repetitions of five unique PRO-FM waveforms and 200 repetitions of one Comp-FM subset of five waveforms, respectively. Both cases provide good target visibility. There also are not appreciable sidelobes in either case, though the dynamic range from the largest target to the noise floor is only about 45 dB and the largest sidelobe in evidence in Fig. 7 was at about −40 dB. Of course, an important take away from this result is that the Comp-FM waveforms are performing well in the presence of Doppler.

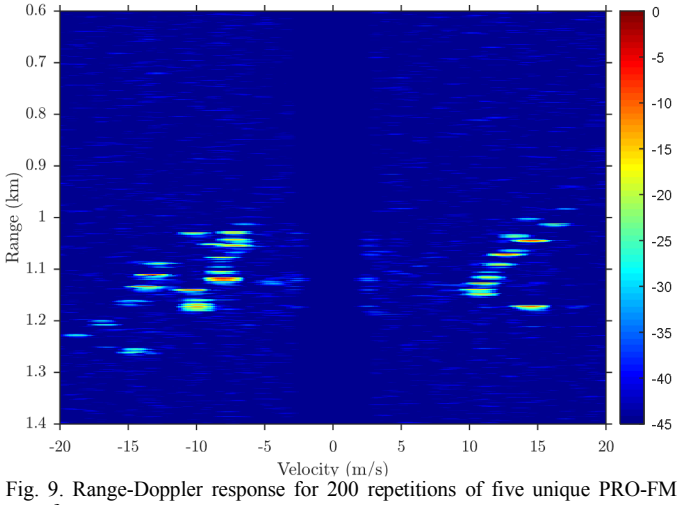

Fig. 9. Range-Doppler response for 200 repetitions of five unique PRO-FM waveforms

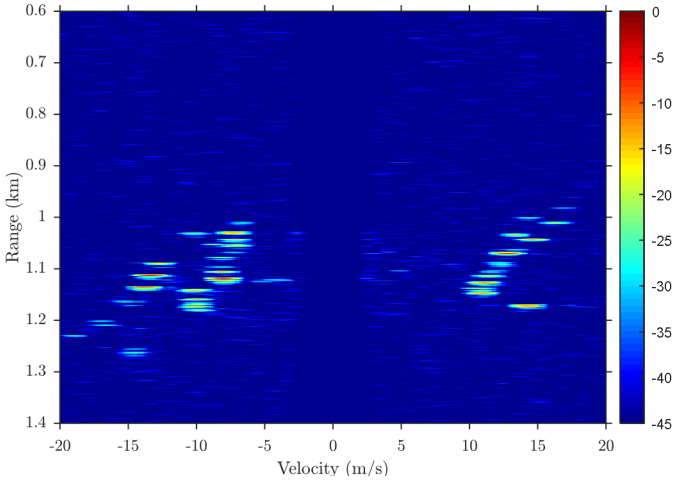

Fig. 10. Range-Doppler response for 200 repetitions of one Comp-FM subset of five waveforms

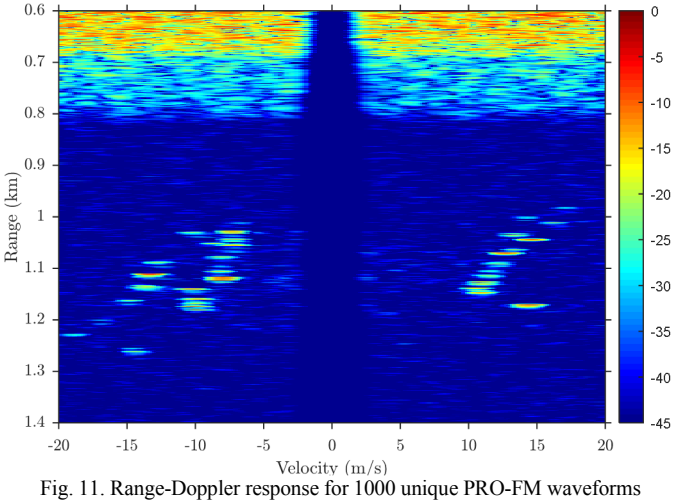

Fig. 11. Range-Doppler response for 1000 unique PRO-FM waveforms

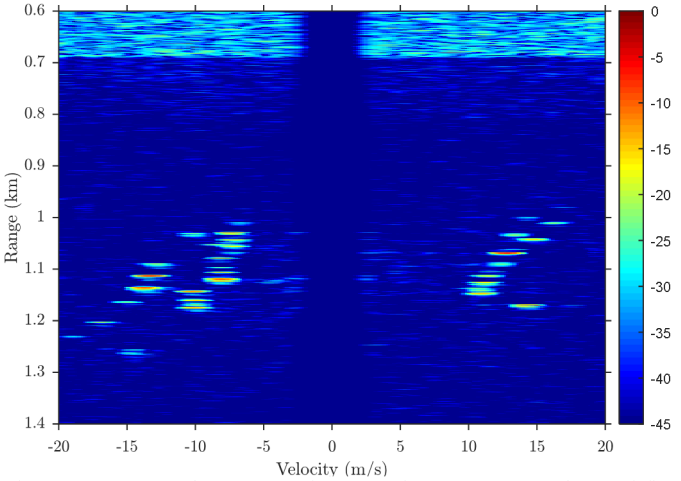

Fig. 12. Range-Doppler response for 200 unique Comp-FM subsets of five waveforms

Finally, Figs. 11 and 12 show the range-Doppler responses for 1000 unique PRO-FM waveforms and 200 unique Comp-FM subsets of 5 waveforms. What is immediately obvious is that, in seeming contradiction to the relationship between Figs. 7 and 8 for the stationary scatterers, these cases have higher sidelobes than the repeated cases of Fig. 9 and 10. However, it should be understood that full pulse agility induces a spreading of clutter sidelobes in Doppler [19-21, 28-30]. This effect can be addressed by either 1) receiver mismatch filtering to further suppress sidelobes [20], 2) a different form of mismatch filtering that "homogenizes" the sidelobes to reduce clutter range sidelobe modulation [28, 31], or 3) simply further increasing the number of pulses to achieve even greater ICS [20].

With that said, the residual clutter around 0.6 to 0.8 km in the Comp-FM case (Fig. 12) is noticeably reduced relative to the PRO-FM case (Fig. 11). This result clearly demonstrates that these Comp-FM waveforms are robust to Doppler effects and, particularly within the FM noise radar context, may be suitable for a variety of radar applications.

VI. Conclusions

The notion of complementary FM waveforms was introduced and demonstrated to be relatively robust to Doppler and transmitter distortion effects. Further, unique subsets of these complementary waveforms are incorporated into a FM noise radar context to enhance capabilities for pulse agility. Waveform design was realized using a fast gradient-based optimization. Both simulation and experimental measurements demonstrate the efficacy of these waveforms that may have utility for a variety of radar applications.

References

[1] M.J.E. Golay, "Complementary series," *IRE Trans. Information Theory*, vol. IT-7, no. 2, pp. 82-87, Apr. 1961.

[2] C.C. Tseng and C.L. Liu, "Complementary sets of sequences," *IEEE Trans. Information Theory*, vol. IT-18, no. 5, pp. 644-652, Sept. 1972.

[3] R. Sivaswamy, "Digital and analog sub-complementary sequences for pulse compression," *IEEE Trans. Aerospace & Electronic Systems*, vol. AES-14, no. 2, pp. 343-350, Mar. 1978.

[4] R. Sivaswamy, "Multiphase complementary codes," *IEEE Trans. Information Theory*, vol. IT-24, no. 5, pp. 546-552, Sept. 1978.

[5] R.L. Frank, "Polyphase complementary codes," *IEEE Trans. Information Theory*, vol. IT-26, no. 6, pp. 641-647, Oct. 1980.

[6] F.F. Kretschmer and K. Gerlach, "Low sidelobe radar waveforms derived from orthogonal matrices," *IEEE Trans. Aerospace & Electronic Systems*, vol. 27, no. 1, pp. 92-102, Jan. 1991.

[7] E. Mozeson and N. Levanon, "Removing autocorrelation sidelobes by overlaying orthogonal coding on any train of identical pulses," *IEEE Trans. Aerospace & Electronic Systems*, vol. 39, no. 2, pp. 583-603, Apr. 2003.

[8] N. Levanon, I. Cohen, P. Itkin, "Complementary pair radar waveforms – evaluating and mitigating some drawbacks," *IEEE Aerospace & Electronic Systems Mag.*, vol. 32, no. 3, pp. 40-50, Mar. 2017.

[9] A. Pezeshki, A.R. Calderbank, W. Moran, and S.D. Howard, "Doppler resilient Golay complementary waveforms," *IEEE Trans. Information Theory*, vol. 54, no. 9, pp. 4254-4266, Sept. 2008.

[10] S.J. Searle, S.D. Howard, and W. Moran, "Formation of ambiguity functions with frequency-separated Golay coded pulses," *IEEE Trans. Aerospace & Electronic Systems*, vol. 45, no. 4, pp. 1580-1597, Oct. 2009.

[11] M. Wicks, E. Mokole, S. Blunt, R. Schneible, V. Amuso, *Principles of Waveform Diversity & Design*, SciTech, 2010, Chap. 48 and Chap. 53.

[12] R.C. Chen and T. Higgins, "Doppler tolerant time separated Golay waveforms," *Intl. Waveform Diversity & Design Conf.*, Kauai, HI, Jan. 2012.

[13] G. Galati, G. Pavan, "Range sidelobes suppression in pulse-compression radar using Golay pairs: some basic limitations for complex targets," *IEEE Trans. Aerospace & Electronic Systems*, vol. 48, no. 3, pp. 2756-2760, July 2012.

[14] H.D. Nguyen, G.E. Coxson, "Doppler tolerance, complementary code sets, and generalised Thue-Morse sequences," *IET Radar, Sonar & Navigation*, vol. 10, no. 9, pp. 1603-1610, Dec. 2016.

[15] S. D. Blunt, M. Cook, J. Jakabosky, J. D. Graaf, and E. Perrins, "Polyphase-coded FM (PCFM) radar waveforms, part I: implementation," *IEEE Trans. Aerospace & Electronic Systems*, vol. 50, no. 3, pp. 2218–2229, July 2014.

[16] S.D. Blunt, E.L. Mokole, "An overview of radar waveform diversity," *IEEE Aerospace & Electronic Systems Mag.*, vol. 31, no. 11, pp. 2-42, Nov. 2016.

[17] P.M. McCormick and S.D. Blunt, "Nonlinear conjugate gradient optimization of polyphase-coded FM radar waveforms," *IEEE Radar Conf.*, Seattle, WA, May 2017.

[18] P.M. McCormick and S.D. Blunt, "Gradient-based coded-FM waveform design using Legendre polynomials," *IET Intl. Radar Conf.*, Belfast, UK, Oct. 2017.

[19] J. Jakabosky, S.D. Blunt, and B. Himed, "Waveform design and receive processing for nonrecurrent nonlinear FMCW radar," *IEEE Intl. Radar Conf.*, Washington, DC, May 2015.

[20] J. Jakabosky, S. D. Blunt, and B. Himed, "Spectral-shape optimized FM noise radar for pulse agility," *IEEE Radar Conf.*, Philadelphia, PA, May 2016.

[21] C.A. Mohr, P.M. McCormick, S.D. Blunt, C. Mott, "Spectrally-efficient FM noise radar waveforms optimized in the logarithmic domain," *IEEE Radar Conf.*, Oklahoma City, OK, Apr. 2018.

[22] J. Jakabosky, S. D. Blunt, B. Himed, "Optimization of 'over-coded' radar waveforms," *IEEE Radar Conf.*, Cincinnatti, OH, May 2014.

[23] B. O'Donnell, J.M. Baden, "Fast gradient descent for multi-objective waveform design," *IEEE Radar Conf.*, Philadelphia, PA, May 2016.

[24] D. Zhao, Y. Wei, Y. Liu, "Spectrum optimization via FFT-based conjugate gradient method for unimodular sequence design," *Signal Processing*, vol. 142, pp. 354-365, Jan. 2018.

[25] E. Ghadimi, R. Feyzmahdavian, M. Johansson, "Global convergence of the heavy-ball method for convex optimization," *European Control Conf.*, Linz, Austria, July 2015.

[26] J. Nocedal and S. Wright, *Numerical optimization*. Springer Science & Business Media, 2006.

[27] P. Zulch, M. Wicks, B. Moran, S. Surova, J. Byrens, "A new complementary waveform technique for radar signals," *IEEE Radar Conf.,* Long Beach, CA, Apr. 2002.

[28] S.D. Blunt, M.R. Cook, J. Stiles, "Embedding information into radar emissions via waveform implementation," *Intl. Waveform Diversity & Design Conf.*, Niagara Falls, Canada, Aug. 2010.

[29] C. Sahin, J. Jakabosky, P. McCormick, J. Metcalf, S. Blunt, "A novel approach for embedding communication symbols into physical radar waveforms," *IEEE Radar Conf.*, Seattle, WA, May 2017.

[30] C. Sahin, J. Metcalf, S. Blunt, "Characterization of range sidelobe modulation arising from radar-embedded communications," *IET Intl. Conf. Radar Systems*, Belfast, UK, Oct. 2017.

[31] C. Sahin, J. Metcalf, S. Blunt, "Filter design to address range sidelobe modulation in transmit-encoded radar-embedded communications," *IEEE Radar Conf.*, Seattle, WA, May 2017.